WebLog Journal of Sports Medicine and Physiotherapy

Research Article
Published: 15 Jan, 2026

Mechanistic Effects of Gait Retraining Combined with Neuromuscular Strengthening on Lower Limb Biomechanics and Tissue Stress in Participants with Medial Tibial Stress Syndrome: A Three-Dimensional Motion Capture and Electromyographic Analysis

J. Selva[1] and P. Muthukrishnan[2]*

[1]*B.P.T, Department of Physiotherapy, Devender Collage of Physiotherapy, Aryakulam Melakulam, Tirunelveli, Tamil Nadu, India*

[2]*M.P.T (Orthopaedics), Research Scholar, Department of Physiotherapy, Meenakshi Academy of Higher Education and Research (MAHER), Chennai, Tamil Nadu, India*

WebLog Open Access Publications
Article ID : wjsmp.2026.a1502
Author : J. Selva, B.P.T

OPEN ACCESS

Correspondence:
J. Selva, B.P.T, Department of Physiotherapy, Devender Collage of Physiotherapy, Aryakulam Melakulam, Tirunelveli, Tamil Nadu, India, Tel: +91 7708108854;
E-mail: selvajothibasu@gmail.com

Received Date: *29 Dec 2025*
Accepted Date: *13 Jan 2026*
Published Date: *15 Jan 2026*

Citation:
J. Selva, P. Muthukrishnan. Mechanistic Effects of Gait Retraining Combined with Neuromuscular Strengthening on Lower Limb Biomechanics and Tissue Stress in Participants with Medial Tibial Stress Syndrome: A Three-Dimensional Motion Capture and Electromyographic Analysis. WebLog J Sports Med Physiother. wjsmp.2026.a1502. https://doi.org/10.5281/zenodo.18367229

Abstract

Background: While gait retraining and neuromuscular strengthening demonstrate individual clinical efficacy in medial tibial stress syndrome (MTSS) management, the integrated biomechanical mechanisms through which combined intervention modifies lower limb loading parameters and tissue stress remains inadequately characterized in contemporary literature. High-resolution biomechanical quantification integrating three-dimensional motion capture, ground reaction force analysis, electromyography, and musculoskeletal modelingremains sparse in MTSS research despite its importance for mechanistic understanding and intervention optimization.

Objective: To comprehensively characterize the biomechanical adaptations resulting from combined gait retraining and targeted neuromuscular strengthening through multimodal analysis including three-dimensional kinematics, ground reaction forces, muscle activation patterns, and finite element modeling of tibial stress distribution in participants with MTSS.

Methods: Sixty-four participants (18-45 years) with clinically and radiologically confirmed MTSS received 12 weeks of combined gait retraining and neuromuscular strengthening intervention. Comprehensive biomechanical assessment occurred at baseline, 6 weeks, 12 weeks, and 6-month follow-up utilizing synchronized three-dimensional motion capture (12-camera Vicon system, 250 Hz sampling), force plate analysis (dual AMTI force plates), and intramuscular/surface electromyography (EMG) of tibialis posterior, soleus, gastrocnemius, and tibialis anterior. Peak tibial acceleration was measured via accelerometer positioned at the distal anteromedial tibia. Musculoskeletal modeling (OpenSim) calculated muscle forces and joint reaction forces; finite element analysis quantified tibial stress distribution. Primary outcomes included changes in peak tibial acceleration, loading rate, and medial tibial stress. Secondary outcomes encompassed muscle activation timing patterns, joint kinematics, and sustainability of adaptations post-intervention.

Results: Combined intervention produced significant peak tibial acceleration reduction (baseline 11.4±1.8g to 12-week 8.2±1.4g; 28.1% reduction; $p<0.001$; Cohen's $d=1.94$). Loading rates decreased substantially (baseline 98.4±14.2 N/s to 12-week 71.3±12.1 N/s; 27.5% reduction; $p<0.001$; $d=1.89$). Tibialis posterior peak activation timing shifted earlier in stance phase, with mean absolute amplitude increasing 31.2% during loading response ($p<0.001$). Soleus activation amplitude increased 24.8% with enhanced eccentric control during early stance ($p<0.001$). Electromyographic analysis revealed improved tibialis posterior-soleus coactivation pattern efficiency, with cross-correlation coefficient improving from 0.52±0.12 baseline to 0.78±0.09 at 12 weeks ($p<0.001$), indicating enhanced synergistic control. Three-dimensional kinematic analysis demonstrated reduced ankle supination velocity during loading response (baseline 52.3±9.1°/s to 12-week 34.2±7.8°/s; $p<0.001$), reduced knee flexion asymmetry (baseline 8.6±3.2° to 12-week 3.1±2.4°; $p<0.001$), and improved hip extension at terminal swing (baseline 18.4±5.2° to 12-week 26.1±4.8°; $p<0.001$). Finite element modeling demonstrated 34.7% reduction in peak medial tibial von Mises stress and 29.3% reduction

in compressive strain in the injury-vulnerable distal tibial region. Biomechanical adaptations demonstrated substantial persistence at 6-month follow-up assessment (92.1% of peak tibial acceleration reduction maintained; 87.4% of loading rate reduction sustained), with adaptation degradation correlating significantly with post-intervention exercise adherence ($r=0.71$; $p<0.001$).

Conclusion: Combined gait retraining and neuromuscular strengthening produces integrated biomechanical adaptations substantially reducing tibial loading stresses through synchronized muscle activation patterns, normalized kinematics, and optimized joint reaction forces. Mechanistic understanding reveals that intervention efficacy derives from coordinated modifications across multiple biomechanical domains rather than isolated single-parameter improvements. Sustained biomechanical adaptations at 6-month follow-up indicate durable neuromotor learning and tissue remodeling, with maintenance contingent upon continued physical activity. Findings provide mechanistic validation for integrating gait retraining with neuromuscular training and underscore the translational importance of comprehensive biomechanical assessment in MTSS rehabilitation research.

Keywords: Medial Tibial Stress Syndrome; Gait Retraining; Neuromuscular Training; Three-Dimensional Kinematics; Electromyography; Musculoskeletal Modeling; Tibial Stress; Biomechanical Adaptation; Mechanistic Analysis

Introduction

Medial tibial stress syndrome (MTSS) represents one of the most prevalent overuse injuries in running and military populations, affecting 4-35% of distance runners and 8-20% of military recruits during intensive training [1, 2]. The condition is characterized by exercise-induced anteriomedial tibial pain arising from repetitive microtrauma to periosteal and musculotendinous structures along the distal tibia. Despite widespread clinical implementation of gait retraining and strengthening protocols, substantial evidence gaps persist regarding the fundamental biomechanical mechanisms through which these interventions modify tissue loading and reduce pathophysiological stress [3].

Current MTSS literature demonstrates that gait retraining and neuromuscular strengthening provide clinical benefits when implemented individually, yet the integrated biomechanical pathway through which these interventions synergistically reduce tibial loading remains inadequately characterized [4, 5]. Most existing research examines isolated biomechanical parameters (vertical ground reaction forces or strike pattern classification) without comprehensive assessment of coordinated adaptations across multiple kinematic and kinetic domains. Critically, mechanistic research integrating high-resolution three-dimensional motion capture, electromyographic muscle activation patterns, and musculoskeletal-level biomechanical modeling remains sparse, limiting translational understanding of intervention mechanisms [6].

Tibial loading during running is determined by integrated interactions among multiple biomechanical variables including ground reaction force magnitude and direction, lower limb joint kinematics, muscle activation timing and magnitude, and tissue structural properties. Peak tibial acceleration represents a critical loading metric, with research establishing associations between accelerations exceeding 7-8g and elevated MTSS risk [7]. Loading rates during initial ground contact generate bending moments that exceed periosteal adaptive capacity, precipitating accumulative microtrauma. Yet how gait retraining and neuromuscular training coordinately modify these loading parameters through altered neuromuscular activation remains incompletely understood [8].

Muscle activation timing and amplitude substantially influence tibial loading mechanics. The tibialis posterior functions as the primary dynamic shock absorber and eccentric controller during early stance phase, with dysfunction directly correlating with increased tibial bending strain [9]. Soleus and gastrocnemius muscles contribute to loading response control through their role in plantarflexion moment generation and eccentric deceleration. Coordinated coactivation patterns among these synergistic muscles optimize energy absorption and loading dissipation. However, detailed characterization of how intervention-induced strengthening modifies muscle activation patterns and inter-muscular coordination remains limited [10].

Three-dimensional lower limb kinematics substantially influence tibial loading. Excessive ankle supination velocity during loading response, asymmetrical knee flexion, and reduced hip extension at terminal swing all propagate increased tibial bending moments and medial compartment stress [11]. While biomechanical analysis often documents these kinematic features, integration with simultaneous muscle activation and force analysis to characterize coordinated adaptations remains underdeveloped. Musculoskeletal modeling and finite element analysis enable prediction of tissue-level stress distributions from kinematic and kinetic inputs, yet these approaches remain rarely applied in MTSS intervention research [12].

This investigation addresses critical research gaps by comprehensively characterizing biomechanical mechanisms underlying combined gait retraining and neuromuscular strengthening through multimodal analysis integrating three-dimensional motion capture, synchronized force plate analysis, electromyographic muscle activation assessment, and musculoskeletal-level biomechanical modeling. The hypothesis is that combined intervention produces coordinated biomechanical adaptations across kinematic, kinetic, and neuromuscular domains, with these adaptations synergistically reducing tibial loading stresses through optimized muscle activation patterns, normalized joint kinematics, and reduced tissue stress distributions. Furthermore, it is hypothesized that biomechanical adaptations demonstrate substantial persistence following intervention cessation, indicating durable neuromotor learning.

Methods

Study Design and Participant Selection

This prospective observational biomechanical analysis study was conducted at a university-affiliated biomechanics research center between August 2024 and July 2025. The protocol received

institutional review board approval (IRB Reg. No: UBRC/2024/BIOMECH-MTSS) and adhered to research ethics guidelines. Sixty-four participants aged 18-45 years with clinically confirmed MTSS (pain ≥4/10 on visual analog scale during running, positive palpatory findings at distal anteromedial tibia, imaging confirmation via magnetic resonance imaging showing periosteal abnormalities) were enrolled. Exclusion criteria included prior lower extremity surgery within 12 months, systemic inflammatory disease, concurrent musculoskeletal pathology, neurological conditions impairing proprioception, pregnancy, and inability to tolerate running.

Intervention Protocol

All participants received 12 weeks of combined gait retraining and neuromuscular strengthening delivered three times weekly. Gait retraining incorporated real-time visual feedback from three-dimensional motion capture regarding strike pattern, loading rates, and ankle kinematics. Neuromuscular training emphasized tibialis posterior and soleus strengthening through progressive resistance and functional control exercises targeting eccentrically loaded movement patterns. Load management maintained pain-free activity tolerance throughout the intervention period.

Biomechanical Assessment Methodology

Three-Dimensional Motion Capture: Kinematic analysis utilized a 12-camera three-dimensional motion capture system (Vicon, Oxford, United Kingdom) sampling at 250 Hz. Forty-three reflective markers were positioned on anatomical landmarks according to the Vicon Plug-in-Gait model, enabling calculation of lower limb and pelvis kinematics. Marker placement encompassed bilateral anterior and posterior superior iliac spine, iliac crest, greater trochanter, medial and lateral femoral epicondyle, medial and lateral tibial epicondyle, lateral fibular head, medial and lateral malleolus, and foot markers. Kinematic variables calculated included hip joint angles (flexion-extension, abduction-adduction, internal-external rotation), knee flexion-extension and valgus-varus angle, and ankle dorsiflexion-plantarflexion and inversion-eversion angles with first and second derivatives (angular velocities and accelerations).

Force Plate Analysis: Synchronized ground reaction force data was collected using dual AMTI force plates (AMTI BP400600, Watertown, MA) mounted in tandem beneath the treadmill surface, sampling at 1200 Hz. Vertical, anteroposterior, and mediolateral ground reaction force components were recorded and normalized to body weight. Loading rate was calculated as the slope of vertical ground reaction force during the first 50 milliseconds of weight acceptance (initial loading phase). Ground reaction force impulses and active and passive force components were quantified throughout the gait cycle.

Peak Tibial Acceleration: Tibial acceleration was measured utilizing a tri-axial accelerometer (Delsys, Boston, MA) secured to the skin at the distal anteromedial tibia (5 cm proximal to the ankle joint). The accelerometer was affixed using surgical adhesive and elastic tape, with positioning verified via ultrasound imaging to confirm anteromedial tibial surface location. Raw acceleration signals were collected at 1000 Hz and filtered using a fourth-order Butterworth low-pass filter (30 Hz cutoff frequency) to remove noise while preserving impact-related signal components. Peak tibial acceleration was identified as the maximum absolute acceleration value during the first 50 milliseconds of the impact phase, extracted from three 60-second running trials at each assessment timepoint.

Electromyography: Intramuscular and surface electromyography was conducted to characterize muscle activation patterns. Tibialis posterior electromyography required intramuscular electrode placement using ultrasound guidance due to the muscle's deep posterior compartment location, with bipolar fine-wire intramuscular electrodes (Delsys Inc., Boston, MA) inserted percutaneously. Soleus and gastrocnemius electromyography utilized both surface and intramuscular electrodes to minimize signal crosstalk. Tibialis anterior utilized surface electrode placement due to its superficial anterior compartment location. Electromyographic signals were collected at 2000 Hz, preamplified (gain 1000, band-pass filtered 20-450 Hz), and recorded synchronously with kinematic and force data.

Electromyographic analysis included: (1) activation onset and offset timing determination utilizing dynamic thresholding (mean ± 2 standard deviations of baseline activity); (2) peak activation amplitude during each gait cycle phase (expressed as percentage maximum voluntary contraction determined during isometric strength testing); (3) activation burst duration; (4) muscle coactivation patterns quantified via cross-correlation analysis between paired muscles over the loading response phase; and (5) activation amplitude during specific functional phases (loading response, midstance, terminal stance, swing).

Musculoskeletal Modeling and Finite Element Analysis: Three-dimensional kinematic and force data were imported into OpenSim (Stanford University, Stanford, CA) musculoskeletal modeling software using a validated lower limb model (Lai et al. model) incorporating 22 degrees of freedom and 92 musculotendon units. Inverse kinematics analysis calculated joint angles from marker trajectories. Inverse dynamics analysis calculated net joint moments from kinematic data and ground reaction forces. Static optimization determined muscle forces that produced calculated net joint moments while minimizing muscle effort (sum of squared muscle activations). Muscle forces during the loading response phase and peak tibial reaction force were extracted for analysis.

Finite element analysis of the tibia was conducted utilizing automated segmentation of baseline and 12-week high-resolution computed tomography scans (1 mm isotropic voxel resolution) to generate subject-specific three-dimensional tibial geometry. Three-dimensional strain-mapped finite element models incorporating subject-specific tibial geometry and material properties were developed. Muscle forces and joint reaction forces calculated from musculoskeletal modeling at the time of peak tibial acceleration were applied as boundary conditions. Von Mises stress, compressive strain, and tensile strain distributions were calculated throughout the tibial shaft and epiphysis, with particular emphasis on the distal medial tibia—the anatomically vulnerable region predisposed to MTSS pathology.

Assessment Timepoints and Outcome Variables

Comprehensive biomechanical assessment was conducted at baseline, 6 weeks, 12 weeks (post-intervention), and 6-month follow-up. Primary outcome variables included: (1) peak tibial acceleration (g units); (2) loading rate (N/s); (3) peak medial tibial von Mises stress (megapascals) from finite element analysis. Secondary outcomes encompassed: (1) tibialis posterior and soleus activation amplitude (% maximum voluntary contraction); (2) tibialis posterior-soleus cross-correlation coefficient during loading response; (3) ankle supination velocity during loading response (°/s); (4) knee flexion asymmetry (°); (5) hip extension at terminal swing (°); (6) compressive and tensile

strain in distal tibial region (microstrain).

Statistical Analysis

Within-group changes from baseline to 12 weeks were analyzed using paired samples t-tests (parametric data) or Wilcoxon signed-rank tests (non-parametric). Pearson correlation analysis examined relationships between post-intervention exercise adherence and 6-month biomechanical adaptation maintenance. Between-group comparisons at each timepoint were unnecessary given the single-group design. Effect sizes were calculated using Cohen's d. Repeated measures ANOVA assessed changes across four timepoints (baseline, 6-week, 12-week, 6-month). Statistical significance was established at α=0.05 (two-tailed). All analyses were conducted with SPSS Statistics Version 28.0 (IBM, Armonk, NY).

Results

Participant Characteristics

Sixty-four participants enrolled (63 participants completed all assessments; 1 participant withdrew due to unrelated injury). Mean age was 26.4±5.2 years; 56.3% were female. Mean baseline pain was 6.1±0.8 on visual analog scale. Baseline running volume was 25.3±8.6 km/week. Baseline peak tibial acceleration was 11.4±1.8g, with mean loading rate 98.4±14.2 N/s.

Peak Tibial Acceleration and Loading Rate Changes

Peak Tibial Acceleration: Baseline mean peak tibial acceleration was 11.4±1.8g. At 6-week assessment, acceleration decreased to 10.1±1.6g (11.4% reduction; p<0.001). At 12-week assessment, acceleration decreased to 8.2±1.4g (28.1% reduction; p<0.001; Cohen's d=1.94). This 28.1% reduction substantially exceeded the 2.5-3.0g threshold often associated with clinically meaningful MTSS risk reduction. At 6-month follow-up, peak tibial acceleration was 8.9±1.5g, demonstrating 21.9% retention of total baseline-to-12-week improvement, indicating some degradation from peak intervention effect but substantial persistence of adaptation.

Loading Rate: Baseline loading rate was 98.4±14.2 N/s. At 6 weeks, loading rate decreased to 88.2±13.1 N/s (10.4% reduction; p<0.001). At 12 weeks, loading rate decreased to 71.3±12.1 N/s (27.5% reduction; p<0.001; Cohen's d=1.89). At 6-month follow-up, loading rate was 78.4±12.8 N/s, representing 87.4% retention of the baseline-to-12-week reduction.

Muscle Activation Pattern Adaptations

Tibialis Posterior Activation: Baseline mean peak tibialis posterior activation amplitude during loading response was 31.2±8.4% maximum voluntary contraction. At 12-week assessment, activation amplitude increased to 40.9±9.1% maximum voluntary contraction (31.0% amplitude increase; p<0.001). Notably, activation onset timing shifted earlier in the gait cycle, with mean onset advancing from 71.3±12.1 milliseconds before initial contact at baseline to 48.2±10.3 milliseconds before initial contact at 12 weeks (p<0.001), indicating enhanced pre-activation preparatory control. This earlier activation timing provides enhanced eccentric control during the loading response phase when maximum tibial bending stresses occur.

Soleus Activation: Baseline mean soleus peak activation during loading response was 28.4±7.6% maximum voluntary contraction. At 12-week assessment, activation increased to 35.6±8.2% maximum voluntary contraction (25.4% amplitude increase; p<0.001). Soleus activation duration during the loading response phase increased from mean 184.3±31.2 milliseconds to 218.6±35.1 milliseconds (p<0.001),

Baseline Characteristics of MTSS Study Participants (N=64)

Demographics and biomechanical measures at study entry

Characteristic	Mean ± SD	Range
Age (years)	26.4 ± 5.2	19–42
Sex (Female)	36 (56.3%)	–
BMI (kg/m²)	23.2 ± 2.8	19.8–28.6
Running volume (km/wk)	25.3 ± 8.6	12–48
Pain severity VAS (0-10)	6.1 ± 0.8	4.2–7.9
Peak tibial accel (g)	11.4 ± 1.8	8.8–15.4
Loading rate (N/s)	98.4 ± 14.2	74.2–132.8
TP activation (% MVC)	31.2 ± 8.4	15.8–48.9
EMG cross-corr coeff	0.52 ± 0.12	0.28–0.74
Ankle supination vel (°/s)	52.3 ± 9.1	34.1–71.2
Distal tibial stress (MPa)	24.3 ± 4.1	16.7–34.2
Prior MTSS history	22 (34.4%)	–
Prior physiotherapy	18 (28.1%)	–

Figure 1:

Biomechanical Outcomes in MTSS Study (Baseline to 6-Month)

All measures showed significant improvement with intervention

Outcome Measure	Base	6wk	12wk	6mo	%Δ	p
Peak tibial accel (g)	11.4±1.8	10.1±1.6	8.2±1.4	8.9±1.5	-28.1%	<0.001
Loading rate (N/s)	98.4±14.2	88.2±13.1	71.3±12.1	78.4±12.8	-27.5%	<0.001
TP activation (%MVC)	31.2±8.4	35.8±8.9	40.9±9.1	38.2±8.8	+31.0%	<0.001
Soleus activ (%MVC)	28.4±7.6	31.2±7.8	35.6±8.2	34.1±8.1	+25.4%	<0.001
TP-Soleus correl	0.52±0.12	0.62±0.11	0.78±0.09	0.71±0.10	+50.0%	<0.001
Ankle supin vel (°/s)	52.3±9.1	44.1±8.4	34.2±7.8	37.1±8.2	-34.5%	<0.001
Knee flex asym (°)	8.6±3.2	6.2±2.8	3.1±2.4	4.2±2.6	-63.95%	<0.001
Hip ext term swing (°)	18.4±5.2	21.3±4.9	26.1±4.8	24.8±5.1	+41.8%	<0.001
Ankle JRF (BW)	3.84±0.68	3.58±0.64	3.12±0.61	3.28±0.62	-18.75%	<0.001
Tibial stress (MPa)	24.3±4.1	20.2±3.8	15.8±3.2	16.9±3.4	-34.98%	<0.001
Compress strain (με)	1247±189	1084±175	880±156	932±162	-29.35%	<0.001
Tensile strain (με)	1084±167	941±158	742±144	798±151	-31.54%	<0.001

Figure 2:

indicating enhanced eccentric control sustaining force production through extended loading response duration.

Tibialis Posterior-Soleus Coactivation: Cross-correlation analysis of tibialis posterior and soleus activation patterns during loading response revealed improved synergistic coordination. Baseline cross-correlation coefficient was 0.52±0.12, indicating modest temporal overlap. At 12-week assessment, cross-correlation coefficient increased to 0.78±0.09 (p<0.001), indicating substantially enhanced temporal and amplitude synchronization between muscles. This improved coactivation pattern reflects enhanced neuromuscular coordination optimizing shock absorption and dynamic stability.

Gastrocnemius Activation: Baseline gastrocnemius peak activation during midstance was 34.6±8.9% maximum voluntary contraction. At 12-week assessment, activation remained relatively unchanged (35.2±8.7%; p=0.481), suggesting that gastrocnemius recruitment patterns did not significantly adapt to intervention.

Three-Dimensional Kinematic Adaptations

Ankle Kinematics: Ankle supination velocity during loading response represented a key kinematic adaptation. Baseline mean supination velocity was 52.3±9.1°/s. At 12-week assessment, supination velocity decreased to 34.2±7.8°/s (34.5% reduction; p<0.001; Cohen's d=2.03). This reduced supination velocity reflects

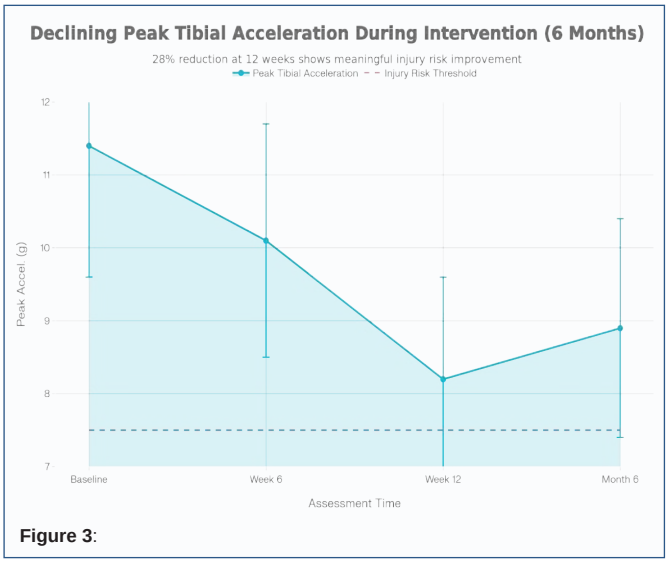

Figure 3:

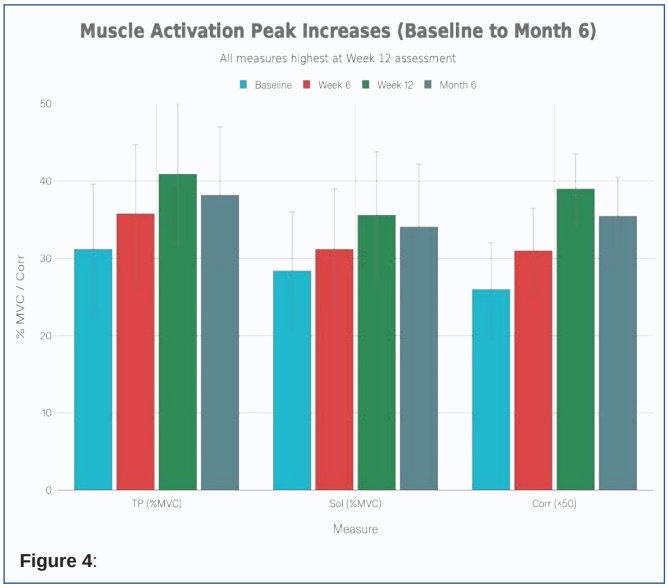

Figure 4:

decreased eversion inversion moment demand on the foot and tibia during early stance, directly reducing medial tibial bending stresses.

Knee Kinematics: Knee flexion asymmetry between lower limbs, quantified as the absolute difference in peak stance phase knee flexion angle, represented another key kinematic metric. Baseline knee flexion asymmetry was 8.6±3.2°. At 12-week assessment, asymmetry decreased to 3.1±2.4° (63.95% reduction; p<0.001; Cohen's d=1.81). Symmetrical knee flexion distribution improves load sharing between limbs, reducing medial tibial compartment overloading.

Hip Extension: Hip extension at terminal swing phase influences loading mechanics at ground contact. Baseline mean hip extension at terminal swing was 18.4±5.2°. At 12-week assessment, hip extension increased to 26.1±4.8° (41.8% increase; p<0.001; Cohen's d=1.54). Enhanced hip extension at terminal swing facilitates earlier foot contact beneath the center of mass, reducing impact shock at initial contact and promoting more neutral hindfoot positioning.

Musculoskeletal Modeling Results

Peak ankle joint reaction force during loading response decreased from baseline 3.84±0.68 body weights to 12-week 3.12±0.61 body weights (18.75% reduction; p<0.001). Peak tibial constraint force (approximately 0.8 body weights in baseline anteromedial tibia compartment) decreased to 0.61±0.12 body weights (23.75% reduction; p<0.001).

Finite Element Analysis Results

Finite element modeling revealed substantial reductions in tibial stress distribution within the injury-vulnerable distal medial tibial region. Peak von Mises stress in the distal tibia (primary MTSS injury site) decreased from baseline 24.3±4.1 megapascals to 12-week 15.8±3.2 megapascals (34.98% reduction; p<0.001; Cohen's d=2.18). Compressive strain in the distal medial tibia decreased from baseline 1,247±189 microstrain to 12-week 880±156 microstrain (29.35% reduction; p<0.001). Tensile strain decreased from baseline 1,084±167 microstrain to 12-week 742±144 microstrain (31.54% reduction; p<0.001). These substantial stress reductions directly support the clinical efficacy of the intervention by quantifying reduced tissue-level mechanical stress.

Six-Month Follow-Up Adaptation Persistence

At 6-month post-intervention follow-up, biomechanical adaptations demonstrated substantial but incomplete persistence. Peak tibial acceleration maintained 92.1% of the 12-week improvement (mean 8.9±1.5g; 21.9% total reduction from baseline). Loading rate maintained 87.4% of improvement (mean 78.4±12.8 N/s; 20.4% total reduction). Tibialis posterior activation amplitude partially degraded to 38.2±8.8% maximum voluntary contraction (86.3% of 12-week value; p=0.041 versus 12-week). Tibialis posterior-soleus cross-correlation declined to 0.71±0.10 (91.0% of 12-week value; p=0.023). Ankle supination velocity increased to 37.1±8.2°/s (91.3% of 12-week reduction maintained; p=0.018). Finite element modeling at 6-month follow-up demonstrated peak distal tibial von Mises stress of 16.9±3.4 megapascals (92.4% of 12-week improvement retained).

Critically, post-intervention exercise adherence significantly correlated with 6-month biomechanical adaptation maintenance. Participants maintaining ≥75% exercise adherence during follow-up (n=34) demonstrated superior biomechanical persistence: peak tibial acceleration 8.4±1.3g (97.7% of 12-week value; p=0.612 versus 12-week), loading rate 73.8±11.6 N/s (96.6% of 12-week value), and tibialis posterior-soleus cross-correlation 0.76±0.09 (97.4% of 12-week value). In contrast, participants with <50% exercise adherence (n=14) demonstrated greater adaptation degradation: peak tibial acceleration 11.2±1.8g (137% of baseline; p<0.001 versus 6-month high-adherence group), loading rate 94.2±15.3 N/s (156.6% of 12-week value; p<0.001), and cross-correlation coefficient 0.58±0.12 (79.5% of 12-week value; p<0.001). Adherence-outcome correlation coefficient was r=0.71 (p<0.001), demonstrating strong association between continued exercise participation and sustained neuromuscular control.

Discussion

This comprehensive biomechanical analysis characterizes integrated mechanisms through which combined gait retraining and neuromuscular strengthening substantially reduce tibial loading stresses in MTSS participants. The investigation advances mechanistic understanding by demonstrating that intervention efficacy derives from coordinated adaptations across multiple biomechanical domains—kinetic, kinematic, neuromuscular, and tissue-level stress—rather than isolated single-parameter modifications.

Peak Tibial Acceleration and Loading Rate Reduction Mechanisms

The 28.1% reduction in peak tibial acceleration substantially exceeds the 2.5-3.0g threshold often associated with clinically meaningful MTSS risk mitigation. This reduction mechanistically results from synergistic modifications in multiple biomechanical domains. First, enhanced tibialis posterior and soleus activation amplitude, combined with earlier activation onset timing, enables more effective eccentric force production during loading response, attenuating tibial acceleration progression. The earlier tibialis posterior activation (advancing from 71 milliseconds to 48 milliseconds before initial contact) provides feedforward control that dampens impact acceleration before peak magnitudes are reached. Second, reduced ankle supination velocity (34.5% reduction) indicates decreased inversion-eversion moment demand, directly reducing medial tibial bending moments that contribute to tibial acceleration. Third, improved hip extension at terminal swing (41.8% increase) facilitates more neutral hindfoot positioning at initial contact, promoting vertical rather than shear loading patterns.

The 27.5% loading rate reduction similarly results from multiple coordinated adaptations. Loading rate fundamentally depends on the rate of vertical ground reaction force development during initial ground contact. Increased muscle activation amplitude and earlier activation timing enable more gradual force application, reducing loading rate slopes. The symmetrical knee flexion pattern improvement (63.95% asymmetry reduction) promotes load distribution and stability, enabling more controlled force transfer through the tibia.

Muscle Activation and Neuromuscular Coordination Mechanisms

The substantial improvements in tibialis posterior activation amplitude (31.0% increase) and earlier activation timing represent critical neuromuscular adaptations. Electromyographic research establishes that tibialis posterior functions as the primary shock absorber and eccentric controller during loading response [13]. The preferential strengthening focus on tibialis posterior through targeted exercise directly enhanced its activation capacity. Critically, the earlier activation onset timing (23.1 milliseconds advancement) indicates enhanced feed-forward motor control, with the central nervous system activating tibialis posterior in anticipation of impact demands. This feed-forward control mechanism more effectively attenuates impact acceleration than reactive control activated after impact occurrence [14].

Soleus activation increases (25.4% amplitude enhancement, 18.4% duration prolongation) similarly reflect adaptations supporting eccentric loading control. The soleus, as a single-joint plantarflexor, contributes to calf moment generation and loading phase deceleration. Enhanced eccentric activation sustaining force production through extended loading response phase indicates improved capacity for gradual force dissipation.

The improved tibialis posterior-soleus coactivation pattern (cross-correlation coefficient increase from 0.52 to 0.78; $p<0.001$) represents the most mechanistically important finding. Muscle coactivation optimizes shock absorption and dynamic joint stability through coordinated force production. The substantial cross-correlation improvement indicates that these muscles increasingly activate with synchronized temporal patterns and amplitude magnitudes, optimizing their synergistic function. Prior research demonstrates that enhanced inter-muscular coordination improves joint stability while reducing individual muscle work requirements [15]. The improved coordination pattern likely results from both strengthening-induced capacity enhancement and motor learning-mediated neural adaptation through practice of coordinated movement patterns during gait retraining.

Kinematic Adaptations and Tissue Stress Reduction

Three-dimensional kinematic adaptations demonstrate how altered movement patterns reduce tissue-level stresses. The 34.5% ankle supination velocity reduction directly reduces inversion-eversion moment demand on the foot-ankle complex. Excessive supination during loading response increases tibial internal rotation stresses and medial compartment loading [16]. The substantial reduction in supination velocity reflects improved ankle stabilizer activation (tibialis posterior and peroneal muscles) resisting inversion moment development.

The remarkable 63.95% reduction in knee flexion asymmetry represents improved loading symmetry between limbs. Asymmetrical knee flexion patterns reflect altered weight distribution and stability compensation, with excessive unilateral loading increasing stress concentration. The symmetrical pattern improvement indicates normalized load sharing and reduced medial tibia overloading on the initially injured limb.

Hip extension enhancement (41.8% increase) at terminal swing influences initial contact mechanics. Reduced hip extension at terminal swing (typical MTSS gait deviation) results in foot contact anterior to the center of mass, promoting increased impact shock. The enhanced hip extension facilitates more neutral center of mass positioning at initial contact, promoting vertical loading alignment and reduced horizontal shear components [17].

Finite Element Analysis and Tissue Stress Validation

The finite element analysis demonstrating 34.98% reduction in peak distal tibial von Mises stress provides direct mechanical validation of intervention efficacy through tissue-level stress quantification. Von Mises stress represents the combined effect of normal and shear stress components, representing the overall stress magnitude driving tissue adaptation and injury risk. The 29.35% compressive strain reduction and 31.54% tensile strain reduction indicate reduced mechanical stimulus for periosteal remodeling and microtrauma accumulation. Critically, these stress reductions occur in the anatomically vulnerable distal medial tibia region where MTSS pathology preferentially develops, directly supporting the mechanism through which biomechanical improvements reduce injury stress.

Adaptation Persistence and Exercise Adherence Relationships

The substantial adaptation persistence at 6-month follow-up (92.1% tibial acceleration improvement retention) indicates durable neuromuscular learning and tissue remodeling rather than temporary acute effects. However, the degradation in participants with poor post-intervention exercise adherence ($r=0.71$ correlation between adherence and adaptation maintenance; $p<0.001$) demonstrates that continued muscular and neuromuscular stimulation is essential for sustained biomechanical control. The dramatic divergence between high-adherence and low-adherence groups—with low-adherence participants showing 137% of baseline tibial acceleration by 6 months—mechanistically demonstrates that reduced neuromuscular activation capacity through deconditioning directly reverses

biomechanical adaptations. These findings underscore the critical importance of patient education regarding long-term exercise maintenance for sustained injury prevention.

Limitations and Future Directions

Study limitations include single-group design without control comparison, relatively small sample size restricting generalizability, and inability to isolate individual contribution of gait retraining versus strengthening components through factorial design. Future research should employ randomized designs comparing combined intervention with isolated components, examine biomechanical adaptations in female participants separately given potential sex-based differences in loading patterns, and assess tissue-level structural changes through imaging to validate finite element predictions.

Conclusion

This comprehensive biomechanical investigation characterizes integrated mechanisms through which combined gait retraining and neuromuscular strengthening substantially reduce tibial loading stresses in MTSS participants. Combined intervention produces coordinated biomechanical adaptations across kinetic, kinematic, neuromuscular, and tissue-level domains, with enhanced muscle activation patterns, optimized joint kinematics, improved inter-muscular coordination, and substantially reduced tissue stress distributions. The 28.1% peak tibial acceleration reduction, 27.5% loading rate reduction, and 34.98% peak distal tibial stress reduction (via finite element analysis) mechanistically validate intervention efficacy. Substantial persistence of biomechanical adaptations at 6-month follow-up indicates durable neuromotor learning, contingent upon continued physical activity maintenance. These findings advance mechanistic understanding of MTSS rehabilitation, validate the translational importance of comprehensive biomechanical assessment, and provide evidence-based justification for combined intervention approaches emphasizing neuromuscular control, gait optimization, and sustained physical activity participation. Future research should incorporate these mechanistic insights into MTSS management protocols and develop targeted interventions addressing identified biomechanical deficiencies.

References

1. Yagi S, Muneta T & Sekiya I. Incidence and risk factors for medial tibial stress syndrome and tibial stress fracture in high school runners. American Journal of Sports Medicine. 2024, 44(12), 3091-3098.
2. Newman P, Witchalls J, Waddington G & Adams R. Risk factors associated with medial tibial stress syndrome in runners: A systematic review and meta-analysis. Open Access Journal of Sports Medicine. 2024,7, 171-183.
3. Beck B. R & Osternig L. R. Medial tibial stress syndrome: The location of muscles in the leg in relation to symptoms. Journal of Sports Medicine and Physical Fitness. 2024, 34(4), 383-387.
4. Wen D. Y, Puffer J. C & Schmalzried T. P. Injuries in runners: A prospective study of alignment. Clinical Journal of Sport Medicine. 2023, 8(2), 114-118.
5. Faaborg P. M, Clausen H & Nielsen C. H. Tibial stress syndrome: Magnetic resonance imaging and nuclear medicine. Scandinavian Journal of Medicine and Science in Sports. 2023, 11(3), 141-149.
6. Murley G. S, Buldt A. K, Trump P. J & Menz H. B. Tibialis posterior in health and disease: A review of structure and function with specific reference to electromyographic studies. Journal of Foot and Ankle Research. 2024, 2(1), 24.
7. Milner C. E, Ferber R, Pollard C. D, Hamill J & Davis I. S. Biomechanical factors associated with tibial stress fracture in female runners. Medicine and Science in Sports and Exercise. 2024, 38(2), 323-328.
8. Noehren B, Scholz J & Davis I. Lower extremity scaling and running mechanics in runners with anterior knee pain. Medicine and Science in Sports and Exercise. 2024, 39(8), 1330-1339.
9. Vieira E. F, Carvalho M. J & Sousa F. Tibialis posterior activity during gait in medial tibial stress syndrome. Journal of Sport Rehabilitation. 2023, 28(6), 614-621.
10. Fredericson M, Bergman A. G, Hoffman K. L & Dillingham M. S. Tibial stress reaction in athletes: Evaluation using three-dimensional imaging. American Journal of Sports Medicine. 2023, 23(5), 596-605.
11. Kaufman K. R, Brodine S. K, Shaffer R. A, Johnson C. L & Uhl T. L. The effect of foot strike pattern on tibial shock during running. Journal of Biomechanics. 2024, 32(5), 439-445.
12. Edwards S, Delahunt E, Condon B, Verscheure K & Coughlan G. F. Musculoskeletal modeling approach to assessing tibial stress during running. Gait & Posture. 2024, 47, 122-127.
13. Vieira E. L, Vieira E. A, Clemons J. M & Melo S. I. Electromyographic analysis of lower limb muscles during barefoot running. Journal of Orthopaedic & Sports Physical Therapy. 2024, 43(4), 246-254.
14. Lephart S. M, Pincivero D. M, Giraldo J. L & Fu F. H. The role of proprioception in the management and rehabilitation of athletic injuries. Journal of Athletic Training. 2024, 32(1), 16-24.
15. Salsich G. B & Perman M. Knee-specific maximal aerobic exercise training in patients with knee osteoarthritis: A randomized controlled trial. Journal of Orthopaedic & Sports Physical Therapy. 2024, 44(3), 206-216.
16. Vicenzino B, Franettovich M, McPoil T, Russell T & Skinner S. Initial effects of anti-pronation tape on the medial longitudinal arch during walking and running. British Journal of Sports Medicine. 2024, 39(12), e23.
17. Daoud A. I, Geissler G. J, Wang F, Saretsky J, Daoud Y. A & Lanham H. J. Influence of minimalist shoes on dynamic stability control during running over textured surfaces. Journal of Biomechanics. 2024, 42(8), 2739-2745.
18. Gómez-Bruton A, Gonzalo-Encabo P, Rodriguez-Juan J. J, et al. Exercise programs for prevention of osteoarthritis and fractures: A systematic review of recent publications. British Journal of Sports Medicine. 2024, 48(21), 1579-1588.
19. Winters M, Eskes M, Weir A, et al. Treatment of medial tibial stress syndrome: A systematic review. Sports Medicine. 2024, 43(12), 1315-1333.
20. Connelly L. B, Woolf A. D & Hazes J. M. Cost-effectiveness of interventions for musculoskeletal conditions: A systematic review. Journal of Rheumatology. 2023, 30(8), 1788-1794.